MNP Enhanced Microwave Imaging by Means of Pseudo-Noise Sensing with Different External Magnetic Field Modulations

Sebastian Ley[1], Bernd Faenger[2], Ingrid Hilger[2] and Marko Helbig[1]

***Abstract*— This contribution deals with the detection and imaging of magnetic modulated nanoparticles by means of ultra-wideband sensing. We performed phantom measurements in a practical measurement setup where the magnetic nanoparticles are modulated by a static and a low periodic changing external magnetic field. We investigated the influence of the modulation type of the polarizing magnetic field on both, detectability and imaging of magnetic nanoparticles. We can conclude that both modulations generate a sufficient contrast in order that the nanoparticles were detected at the correct position in a three-dimensional volume. The imaging results, including 32 channels, indicate that the two state (ON/OFF) modulation of the magnetic field under constant environmental conditions shows better results compared to a sinusoidal excitation of the magnetic field.**

I. INTRODUCTION

Magnetic nanoparticles (MNPs) are of great interest for a variety of biomedical applications, e.g. as contrast agent for cancer detection, in which the MNPs bind specifically to tumor cells. Therefore, the knowledge of the presence and the spatial distribution of the MNPs inside of an organism is essential for a reliable detection of cancer cells. There are different technologies, which exploit the magnetic properties of MNP to detect and image them, such as MRI [1], Magnetic Particle Imaging (MPI) [2] and Magnetorelaxometry (MRX) [3].

A further promising approach is the contrast enhanced microwave imaging [4], [5] where the detection of MNPs are based on a differential measurement. A transmitting antenna emits electromagnetic waves into the medium under test (MUT). The electromagnetic waves are partially reflected at each dielectric and magnetic boundary. The scattered electromagnetic waves are captured by receiving antennas. In order to eliminate the undesired clutter (e.g. antenna crosstalk) and to detect the MNPs, a differential measurement between the OFF and ON state of a polarizing magnetic field (PMF) is performed. Supposing that an amount of functionalized MNPs has accumulated in the tumor, their magnetic properties can be modulated by the external PMF. This results in a changing scattering behavior, which can be detected by means of microwave sensing. The surrounding tissues are not affected by the PMF due to their non-magnetic properties.

In this work, we investigated the influence of the type of PMF modulation on the MNP detection and imaging results using UWB sensing. Phantom measurements were performed with an ON/OFF modulation of the PMF as described in [5] and a periodical sinusoidal modulation as suggested in [6]. The results were compared and discussed regarding to a practical application.

II. MATERIALS AND METHODS

A. UWB M-sequence radar

The UWB measurements were performed applying the M-sequence sensor technology, which was developed at Technische Universität Ilmenau. This correlation measurement approach uses a binary pseudo-noise code (M-sequence) to stimulate the medium under test (MUT). The M-sequence is generated by a binary high-speed shift register. The impulse response function (IRF) of the MUT is computed by the cross correlation of the stimulus signal and the received signal. A detailed description of the M-sequence working principle is given by Sachs [7].

B. Measurement setup

The measurement setup is based on our previous work presented in [5]. It consists of an electromagnet with an air gap of approximately 14 cm. The electromagnet is operated with a voltage source (EAC-S 3000, ET System electronic GmbH, Germany). An antenna array which holds the active dipole antennas (bowtie) is placed in the air gap as shown in Fig. 1. We used a two-channel UWB radar with a bandwidth of 5 GHz containing one transmitter (Tx) and two receivers (Rx). In order to increase the number of channels, we simulate an antenna rotation by rotating the breast phantom in steps of 22.5° which results in a total number of 32 channels.

The phantom consists of a mixture of 96 wt./wt. % distilled water and 4 wt./wt. % agar. The target is a 3D printed hollow sphere with a total volume of 2 mL. It is filled with 20 mg of MNPs (WHKS 1S12, Liquids Research Limited, Bangor, UK) diluted in distilled water. The target is embedded in the agar phantom as depicted in Fig. 1.

C. Signal processing and MNP detection

Fig. 2a shows the raw radargram exemplarily for an ON/OFF measurement where each column corresponds to a measured impulse response function (IRF). The sample rate is approximately 5 IRFs per second. It is obvious that

*This work was supported by the German Research Foundation (DFG) in the framework of the project ultraMAMMA II (HE 6015/1-3).

[1] Sebastian Ley and Marko Helbig are with the Faculty of Computer Science and Automation, Institute of Biomedical Engineering and Informatics, Technische Universität Ilmenau, 98693 Ilmenau, Germany sebastian.ley@tu-ilmenau.de

[2] Bernd Faenger and Ingrid Hilger are with the Institute of Diagnostic and Interventional Radiology, Jena University Hospital, Friedrich Schiller University, Jena, Germany

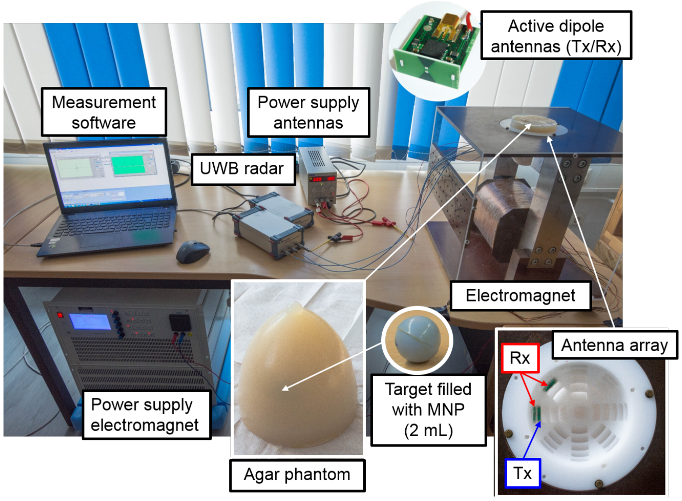

Fig. 1. Measurement setup for MNP detection and imaging. The agar phantom with the target inside is placed in the air gap of the electromagnet. Small active dipole antennas and an UWB M-sequence radar system are applied for measurements.

the MNP response is superimposed by clutter (e.g. antenna crosstalk). In the following, MOD indicates the type of PMF modulation. We applied an ON/OFF modulation (ONOFF) and a sinusoidal modulation (SIN) with a modulation frequency of $\nu_m = 0.5\,Hz$ of the PMF . The equations below are valid for both modulation approaches. In order to eliminate the undesired reflections, we performed a differential measurement by subtracting the mean IRF ($\overline{x}_{MOD,T_{OFF}}(t)$) column by column from the raw radargram $x_{MOD}(t,T)$:

$$y_{MOD}(t,T) = x_{MOD}(t,T) - \overline{x}_{MOD,T_{OFF}}(t), \tag{1}$$

where t is the propagation time, T is the observation time and

$$\overline{x}_{MOD,T_{OFF}}(t) = \frac{1}{T_{OFF}} \int_{T_{OFF}} x_{MOD}(t,T)\,dT \tag{2}$$

indicates the estimated static signal components. The magnetic field intensity in the air gap is defined by the current flowing through the coil. Therefore, we set the amplitude of the current to $I = 9\ A$ during T_{ON} for ON/OFF analysis. To compare both modulation approaches the root mean square (RMS) current for the SIN modulation was $I_{RMS} = 9\ A$.
Fig. 2b and Fig. 3b represent the clutter removed radargrams $y_{ONOFF}(t,T)$ and $y_{SIN}(t,T)$ with the corresponding PMF modulated MNP response. The MNP response in terms of ON/OFF modulation shows a constant amplitude in the radargram during the presence of the PMF (T_{ON}) as depicted in Fig. 2b and in the case of the SIN modulation, the MNP response has a periodic shape during T_{ON} as shown in Fig. 3b.
After clutter elimination we computed the Fourier Transform of $y_{MOD}(t,T)$ in observation time over the time period with the presence of the PMF

$$Y_{MOD}(t,\nu) = \frac{1}{T_{ON}} \int_{T_{ON}} y_{MOD}(t,T) \cdot e^{-j2\pi\nu T}\,dT \tag{3}$$

to extract the MNP response in the frequency domain. Considering the ON/OFF modulation approach, the MNP response corresponds to the steady component ($\nu = 0$) of the spectrum as shown in Fig. 2c. In the case of SIN modulation it should be noticed that the periodic shape of the MNP response (see Fig. 3b) corresponds to the absolute value function of a sine wave. This results in a MNP response occurring at $\nu = 0\,Hz$ (steady component) and at the second harmonic $\nu = 2 \cdot \nu_m = 1\,Hz$ as shown in Fig. 3c.

III. MNP Imaging

In terms of the imaging process, the input signal is defined by

$$y_{MOD}(t) = \left|Y_{MOD}(t,\nu)\right|, \tag{4}$$

with $\nu = 0\,Hz$ (steady component) considering the ON/OFF modulation and $\nu = 1\,Hz$ in terms of the SIN modulation. The signal $y_{MOD}(t)$ corresponds to one measured channel and if we consider a number of channels n we can apply the delay-and-sum (DAS) algorithm to compute an image as described in literature (e.g. [8]). The image processing is realized in time domain as follows

$$I(\mathbf{r}_0) = \left(\sum_{n=1}^{N} \left|y_{n,MOD}(\tau_n(\mathbf{r}_0))\right|\right)^2 \tag{5}$$

where N is the number of channels, $\mathbf{r}_0$ represents the coordinates of the focal point and $\tau_n(\mathbf{r}_0)$ is the focal point dependent time delay of channel n.

Fig. 4b and Fig. 5b show the results for the 2 mL target including 20 mg MNPs for the ON/OFF and the SIN modulation, respectively. Furthermore, we computed a reference image for each modulation approach without the presence of a PMF as depicted in Fig. 4a and Fig. 5a. To compare the images we introduce a signal to reference signal ratio S/S_{ref} where S is the mean intensity of the target region with the presence of the PMF (Fig. 4b and Fig. 5b) and S_{ref} is the mean intensity of the target region without the presence of the PMF (Fig. 4a and Fig. 5a). The center of the 2 mL spherical volume is located at $[x,y,z] = [0\,cm, 2.5\,cm, -3\,cm]$. Tab. I summarizes the S/S_{ref} ratios for ON/OFF and SIN modulation. In addition to the MNP response of the SIN modulation at $1\,Hz$, we have also considered the steady component ($\nu = 0\,Hz$) as well as the target response including both frequencies (0 and $1\,Hz$).

TABLE I
S/S_{ref} for ON/OFF and SIN modulation

PMF	ON/OFF	SIN		
ν	0 Hz	0 Hz	1 Hz	0 Hz + 1 Hz
S/S_{ref}	13.5 dB	12.3 dB	6.4 dB	10.5 dB

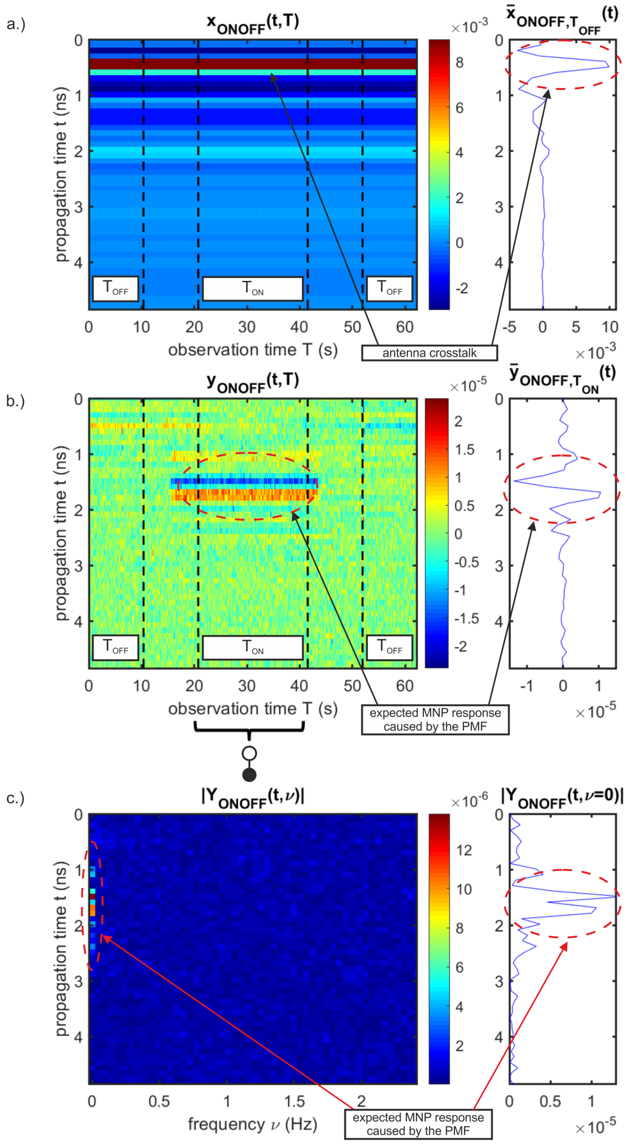

Fig. 2. ON/OFF modulation a.) Raw radargram $x_{ONOFF}(t,T)$ and the corresponding mean IRF $\overline{x}_{ONOFF,T_{OFF}}(t)$ averaged over the time period without the presence of the external PMF, b.) Clutter removed radargram, c.) Single sided magnitude spectrum with the extracted MNP response $|Y_{ONOFF}(t,\nu=0)|$ (right)

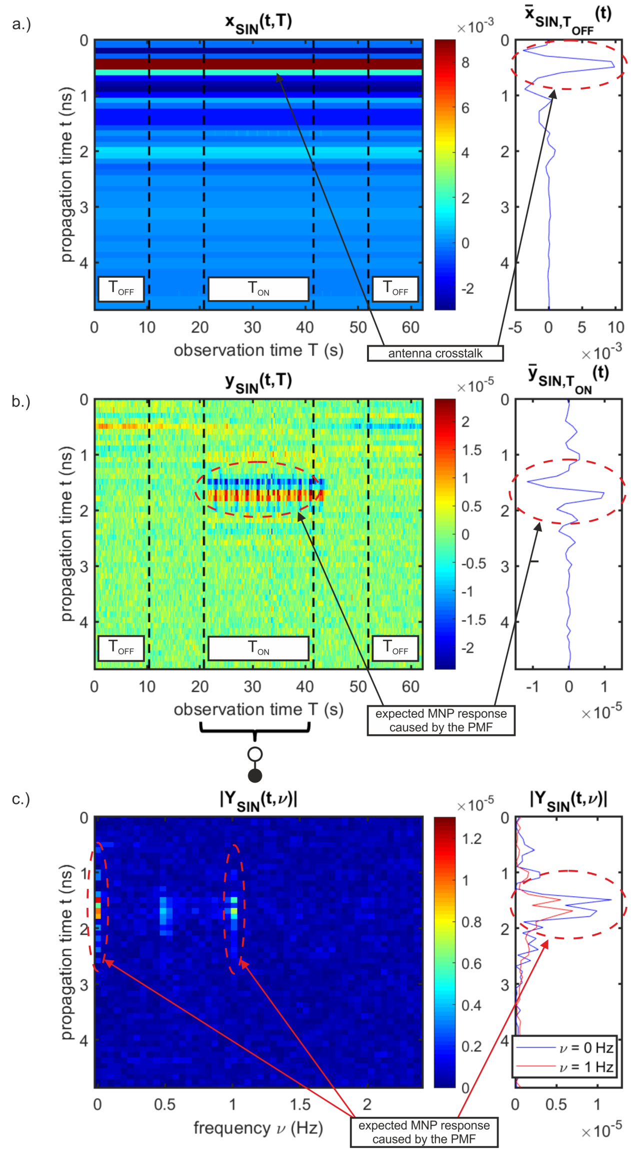

Fig. 3. SIN modulation a.) Raw radargram $x_{SIN}(t,T)$ and the corresponding mean IRF $\overline{x}_{SIN,T_{OFF}}(t)$ averaged over the time period without the presence of the external PMF, b.) Clutter removed radargram, c.) Single sided magnitude spectrum $|Y_{SIN}(t,\nu)|$ and the extracted MNP responses for $\nu = 0\,Hz$ and $\nu = 1\,Hz$ (right)

IV. DISCUSSION AND CONCLUSION

In this paper we investigated the influence of the type of PMF modulation on the detectability and imaging of MNPs in a realistic measurement setup. We analyzed an ON/OFF modulation and a SIN modulation of the PMF under comparable conditions. To ensure comparability, the supply current of the electromagnet was determined by its RMS value ($I_{RMS} = 9\,A$) for both cases. The results indicate that the particles were successfully detected with both approaches, whereby the ON/OFF modulation shows a higher S/S_{ref}. The limited spatial resolution of the MNPs, especially in z-direction, can be explained by the small number of channels. Regarding the SIN modulation, the MNP response does not show a sine curve but its absolute value function. This results in a steady component as well as in a second harmonic of the modulation frequency ν_m as shown in Fig. 3c. If we only consider the second harmonic ($\nu = 1\,Hz$) of $|Y_{SIN}(t,\nu)|$ for imaging, this results in a lower S/S_{ref} compared to the ON/OFF modulation as shown in Fig. 5.

A further advantage of the ON/OFF modulation is the fact that the two states of the PMF can be chosen with respect to the optimal magnetic field intensities of $0\,kA/m$ and $80\,kA/m$ as described by Bellizzi et al. [9]. The phantom experiments show only slight drift effects due to the nearly constant environmental conditions during the measurements. Concerning a practical measurement setup with patients, additional drift effects (minimal patient movement, sweat)

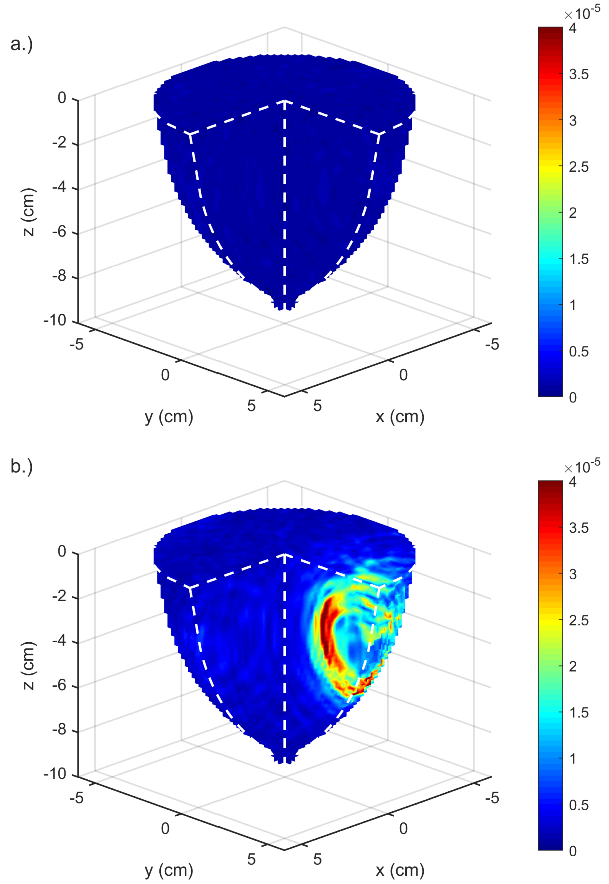

Fig. 4. 3D UWB images based on differential measurements with a 2 mL target including 20 mg of MNPs, a.) without the presence of a PMF, b.) with ON/OFF modulation of the PMF

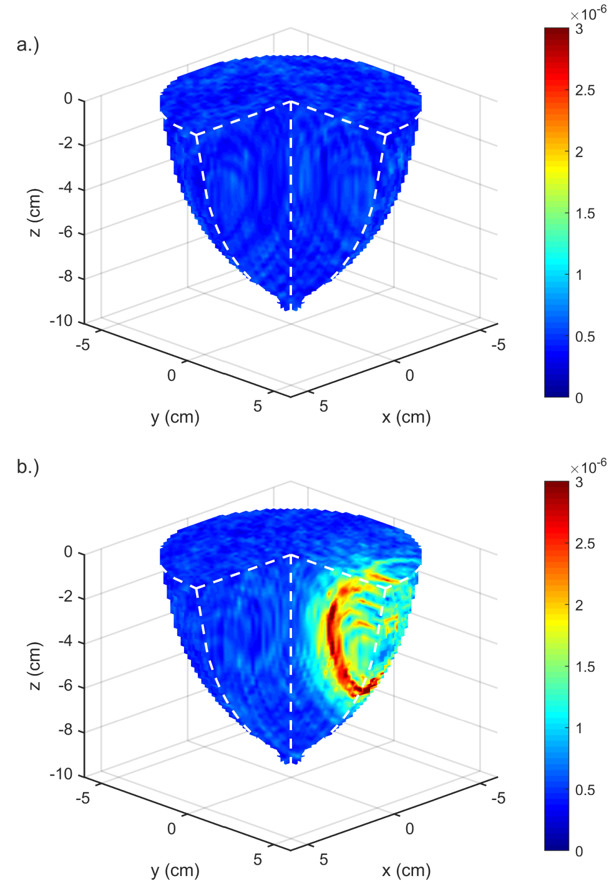

Fig. 5. 3D UWB images based on differential measurements with a 2 mL target including 20 mg of MNPs, DAS beamforming based on the second harmonic $\nu = 1\,Hz$, a.) without the presence of a PMF, b.) with sinusoidal modulation of the PMF

can influence the results. Considering such a case, drift effects have to be analyzed in order to determine the correct MNP response. Regarding the ON/OFF modulation, a linear drift in observation time will not affect the steady component, because it will be eliminated during the clutter removal (see eq. (1)). However, if the drift has a non-linear trend, low frequencies and the steady component are more affected and in that case the SIN modulation with an appropriate high modulation frequency ν_m can improve the detection and imaging results as well. This will be investigated in future work.

References

[1] Q. A. Pankhurst, J. Connolly, S. K. Jones and J. Dobson, Applications of magnetic nanoparticles in biomedicine, Journal of Physics D: Applied Physics, vol. 36, no. 13, pp. 167-181, 2003.

[2] J. Weizenecker, B. Gleich, J. Rahmer, H. Dahnke and J. Borgert, Three-dimensional real-time in vivo magnetic particle imaging, Physics in Medicine and Biology, vol. 54, no. 5, pp. 1-10, 2009.

[3] F. Wiekhorst, U. Steinhoff, D. Eberbeck and L. Trahms, Magnetorelaxometry Assisting Biomedical Applications of Magnetic Nanoparticles, Pharmaceutical Research, vol. 29, pp. 11891202, 2012.

[4] G. Bellizzi, O. M. Bucci and I. Catapano, Microwave Cancer Imaging Exploiting Magnetic Nanoparticles as Contrast Agent, IEEE Transactions on Biomedical Engineering, vol. 58, no. 9, pp. 2528-2536, 2011.

[5] S. Ley, M. Helbig, and J. Sachs, MNP enhanced microwave breast cancer imaging based on ultra-wideband pseudo-noise sensing, Proc. European Conference on Antennas and Propagation (EuCAP) 2017, Paris, France, pp. 2754-2757, 2017.

[6] S. Ley, M. Helbig, J. Sachs, S. Frick and I. Hilger., First trials towards contrast enhanced microwave breast cancer detection by magnetic modulated nanoparticles, Proc. European Conference on Antennas and Propagation (EuCAP) 2015, Lisbon, Portugal, pp. 1-4, 2015.

[7] J. Sachs, Handbook of Ultra-Wideband Short-Range Sensing: Theory, Sensors, Applications, Wiley-VCH, Berlin, 2012.

[8] E. C. Fear, X. Li, S. C. Hagness and M. A. Stuchly, Confocal Microwave Imaging for Breast Cancer Detection: Localization of Tumors in Three Dimensions, IEEE Transactions on Biomedical Engineering, vol. 49, no. 8, pp. 812-822, 2002.

[9] G. Bellizzi, G. G. Bellizzi, O. M. Bucci, L. Crocco, M. Helbig, S. Ley and J. Sachs, Optimization of the Working Conditions for Magnetic Nanoparticle-Enhanced Microwave Diagnostics of Breast Cancer, IEEE Transactions on Biomedical Engineering, vol. 65, no. 7, pp. 1607-1616, 2018.